9th Int. Conference on Nuclear Engineering – ICONE-9
Nice, France, April 8 - 12, 2001
ICONE-9683

A NUMERICAL APPROACH TO THE SIMULATION OF ONE-PHASE AND TWO-PHASE REACTOR COOLANT FLOW AROUND NUCLEAR FUEL SPACERS

Zoran V. Stosic and Vladimir D. Stevanovic[1]

Framatome ANP GmbH - NBTT
Bunsenstr. 43, D-91058 Erlangen, Germany
E-mail: Zoran.Stosic@Framatome-ANP.de

A methodology for the simulation and analysis of one-phase and two-phase coolant flows around one or a row of spacers is presented. It is based on the multidimensional two-fluid mass, momentum and energy balance equations and application of adequate turbulence models. Necessary closure laws for interfacial transfer processes are presented. The stated general approach enables simulation and analyses of reactor coolant flow around spacers on different scale levels of the rod bundle geometry: detailed modelling of coolant flow around spacers and investigation of the influence of spacer's geometry on the coolant thermal-hydraulics, as well as prediction of global thermal-hydraulic parameters within the whole rod bundle with the investigation of the influence of rows of spacers on the bulk thermal-hydraulic processes. Sample problems are included illustrating these different modelling approaches.

Keywords: Two-phase, Flow, Simulations

1. INTRODUCTION

Spacers are built into nuclear fuel bundles to support thin structure of fuel rods, but they also have positive effects on enhancement of heat transfer and increase of the critical heat flux (CHF) [1,2]. The enhancement of the heat transfer is achieved by the formation of recirculation zones behind and around the spacer, intensive flow mixing and phase separation. Hence, there is a strong interest to get insight into these processes. The investigation of these effects can be efficiently supported with the numerical simulation of the turbulent multidimensional reactor coolant flow around spacers. Results of the numerical simulations are used in safety analyses, as experimental pre-tests calculations, for the evaluation of measured data, in a rod bundle design procedure. Thoroughly verified and assessed numerical model can even lead to the removal of a need for experimental work in certain ranges of process parameters and thermal-hydraulic conditions.

A methodology, based on the numerical solution of the multidimensional two-fluid model of reactor coolant flow, and on the application of the appropriate form of the k-ε turbulence model, is presented in the paper. Numerical solution algorithm is based on the control volume approach. The paper presents numerical solution strategy, applied fluid dynamics and thermal-hydraulics models, numerical schemes and some sample problems. Presented simulation and modelling methodology is used for an investigation of the influence of spacers' geometry and positions onto the coolant thermal-hydraulics in [3]. Also, this methodology is applied for the investigation of the phase separation in two-phase flows over spacers [4].

2. PHYSICAL MODELS

A complexity of the reactor coolant flow around spacers has introduced several physical models which enables efficient modelling investigation of the spacers influence on the reactor thermal-hydraulics. From the standpoint of the coolant thermo-physical state there is a need to consider both one-phase coolant flow and two-phase steam-water flow around spacers. Also, two types of flow channel models are considered. The first ones are formed by rod and spacers of different geometry and shapes. These solid walls are physical boundaries of the investigated flow channels and no-slip

[1] Temporarily at Framatome ANP GmbH, P.O.Box 3220, D-91050 Erlangen, Germany

velocity conditions are prescribed for these boundaries. This representation enables detailed investigation of the coolant flow around spacers, which comprises the investigation of the influence of spacer's geometry on recirculation zones formation, phases separation, flow resistance, pressure drops etc. Unfortunately, such detailed spacers and rods geometry modelling is not practical for engineering purposes when the whole rod bundle thermal-hydraulic is investigated. The presence of several spacer rows, at several levels along the bundle height, as well as number of spacers and rods, make it practically impossible to perform detailed simulation of coolant flow around every bundle element. Because of this, the second approach to spacers and rod bundle geometry modelling is introduced, based on the porous media concept. By this approach, the coolant flow around rods and spacers is observed as a flow through the flow channel with volumetrically distributed flow resistance, while this flow resistance is determined by the rods and spacers geometry and spatial distribution. Reactor coolant flow parameters, predicted by the application of the porous media concept, represent volume averaged parameters. They quantify the large scale thermal-hydraulic processes within the rod bundle, but they do not represent the fine flow micro structure around every rod or spacer. A unique model, able to consider these diverse modelling requirements, is presented in the following sections.

3. GOVERNING EQUATIONS

Three-dimensional liquid and vapour two-phase flow is modelled by the "two fluid" model [5]. Mass, momentum and energy fluid flow conservation equations are written for both phases. The general form of the conservation equations takes into account the possibility of two-phase flow around rods in a bundle through the application of the porous-media concept. Mass, momentum and energy transfer at the vapour-liquid interface, as well as rod bundle hydraulic resistance to two-phase flow, heat transfer from hot rods and boiling within a rod bundle are modelled by "closure laws". This approach implies nonequilibrium thermal and flow conditions. The following assumptions are introduced:

- The porous medium concept is used in the simulation of two-phase flow within a rod bundle. The space of the numerical control volume can be occupied by one or both phases – vapour and liquid, as well as by rods. The flow volume reduction due to the presence of rods in a space occupied by a bundle is taken into account. Therefore, the conservation of the vapour and liquid flow parameters is performed only for the fractions of the numerical control volume occupied by corresponding phase.
- A rod bundle flow resistance is assumed to be continuously distributed in the space occupied by these elements.
- Flow governing equations are written in the nonviscous form, while the turbulent viscosity effects are taken into account indirectly through friction coefficients for the rod bundles flow resistance and two-phase interfacial drag force.
- The two-phase flow is observed as semi-compressible, that is the acoustic flow effects are neglected, while the influence of the pressure change on the vapour and liquid thermo-physical properties is taken into account.
- The surface tension is neglected as it is not important for bulk two-phase flow phenomena. Hence, pressure is the same for both phases within the numerical control volume.

Conservation equations take the following form in the indicial notation.

Continuity equation

$$\frac{\partial \alpha_k \rho_k}{\partial t} + \frac{\partial \left(\alpha_k \rho_k u_{k,i}\right)}{\partial x_i} = (-1)^k (\Gamma_e - \Gamma_c) \tag{1}$$

Momentum balance

$$\frac{\partial \left(\alpha_k \rho_k u_{k,i}\right)}{\partial t} + \frac{\partial \left(\alpha_k \rho_k u_{k,i} u_{k,j}\right)}{\partial x_j} =$$

$$-\alpha_k \frac{\partial p}{\partial x_i} + \frac{\partial}{\partial x_j}\left[\alpha_k (\rho_k \eta_k \frac{\partial u_{k,i}}{\partial x_j} - \rho_k \overline{u'_{k,i} u'_{k,j}})\right] + \alpha_k \rho_k g_i + (-1)^k (\Gamma_e - \Gamma_c) u_{ik,i} + \tag{2}$$

$$(-1)^k F_{L2,i} + (-1)^{k+1} F_{VM,i} + (-1)^{k+1} F_{21,i} - F_{3k,i}$$

Scalar flow parameter conservation

$$\frac{\partial(\alpha_k \rho_k h_k)}{\partial t} + \frac{\partial(\alpha_k \rho_k u_{k,i} h_k)}{\partial x_i} = \frac{\partial}{\partial x_i}\left[k_k \frac{\partial T_k}{\partial x_i} - \rho_k c_{p_k} \overline{T_k' u_{k,i}'}\right] + (-1)^k (\Gamma_e - \Gamma_c) h'' + q_{3k}''' \quad (3)$$

Parameters u, p, T are time averaged instantaneous velocity, pressure and temperature, respectively. Instantaneous parameters are represented as the sums of the time averaged parameters and the turbulent fluctuating components

$$\hat{u}_{k,i} = u_{k,i} + u_{k,i}', \quad \hat{p} = p + p', \quad \hat{T}_k = T_k + T_k' \quad (4)$$

As the consequence of the instantaneous equations time averaging the following terms appear

$$\overline{u_{k,i}' u_{k,j}'} \text{ and } \overline{u_{k,i}' T} \quad (5)$$

which represent the Reynolds stress tensor and the turbulent heat flux vector. The index k is 1 for water and 2 for steam. The source terms for mass, momentum and thermal energy conservation are written on the r.h.s. of Eqs. (1)-(3). The term $\rho_k \overline{u_{k,i}' u_{k,j}'}$ in Eq. (2) represents turbulent stress in phase k. The intensity of phase transition, which is the mass of evaporation or condensation per unit volume and time, are denoted with Γ_e and Γ_c respectively. The force of vapour and liquid interfacial drag per unit volume in i Cartesian direction is denoted with $F_{21,i}$, while the forces of rods resistance to liquid and vapour flow within a bundle, per unit volume, are represented with $F_{3k,i}$. Terms $F_{L2,i}$ and $F_{VM,i}$ represent lift force and virtual mass force, respectively. The term q_{3k}''' represents volumetric heat rate from rods to corresponding fluid phase per unit volume.

In case of two-phase flow within a rod bundle the following volume fraction balance holds

$$\alpha_1 + \alpha_2 + \alpha_3 = 1 \quad (6)$$

while for two-phase flow in a free channel the following balance is valid

$$\alpha_1 + \alpha_2 = 1 \quad (7)$$

4. CONSTITUTIVE CORRELATIONS

Geometric relations. The rods or spacers volume fractions are determined according to their geometry and dimensions. For instance, rods volume fraction α_3 is calculated according to the defined arrangement of the rods in the bundle, Fig. 1.

Vapour-liquid flow patterns. The vapour volume fraction in the two-phase mixture (void) is determined according to the following expression

Rods *volume fraction* α_3

$$\alpha_3 = \frac{\pi}{4} \frac{D^2}{P_x P_y}$$

Porosity

$$\psi = 1 - \alpha_3$$

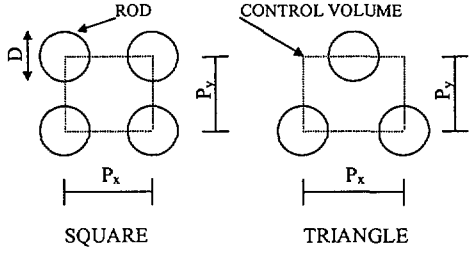

Figure 1 Geometric parameters for rod bundle description

$$\varphi = \alpha_2/(\alpha_1 + \alpha_2). \tag{8}$$

Although the multidimensional two-fluid model is able to predict phase separation and spatial phase distribution, there is still a need for two-phase flow pattern pre-assumption.

Some experimental evidence about the two-phase flow patterns within rod bundles [6] has led to a simple assumption about the two-phase flow patterns, as it is presented in Table 1.

Table 1: Two-phase flow pattern prediction

Bubbly flow	Churn-turbulent flow	Annular and/or mist flow
$\varphi \leq 0.3$	$\varphi > 0.3$ *and* $(\varphi \vec{u}_2) < 15 m/s$	$\varphi > 0.3$ *and* $(\varphi \vec{u}_2) > 15 m/s$

For two-phase flows in free flow channels (without volumetrically distributed flow resistance) an appropriate two-phase flow pattern map should be used, as the Bennett map for two-phase vertical channel flow [7].

Interfacial drag force. Calculation of the interfacial drag force ($\vec{F}_{21}$) is a crucial step for the proper prediction of the relative velocities between vapour and liquid phase, and consequently the void fraction. The interfacial drag force per unit volume of computational cell, which can be filled with liquid, vapour and tubes, or only with vapour and liquid, is calculated as

$$F_{21,i} = \frac{3}{4}\alpha_2 \rho_1 \frac{C_D}{D_p} \sqrt{\sum_{j=1}^{3} (u_{2,j} - u_{1,j})^2}\,(u_{2,i} - u_{1,i}), \tag{9}$$

where C_D is the interfacial drag coefficient, and D_p is the diameter of the dispersed particle.

Interfacial drag coefficient for two-phase flow within tube bundles. Correlations for the interfacial drag coefficient C_D are tested for flows inside tubes, while limited information is available in the literature about the prediction of C_D for two-phase flows within vertical or horizontal rod bundles. Therefore, for bubbly two-phase flow within a rod bundle, the Ishii-Zuber correlation [8], developed for a distorted particle two-phase flow inside a tube, is adopted for the calculation of C_D. The original correlation is multiplied with 0.4, Eq. (10). This could be attributed to the fact that due to the presence of tubes/rods in the bundle, the vapour-liquid interface is more distorted, what leads to the lower value of the interfacial drag coefficient C_D.

$$C_D = 0.267 D_p \left(\frac{g\Delta\rho}{\sigma}\right)^{1/2} \left\{\frac{1 + 17.67 f(\varphi)^{6/7}}{18.67 f(\varphi)}\right\}^2 \tag{10}$$

where

$$f(\varphi) = (1 - \varphi)^{1.5}, \tag{11}$$

and void fraction in two-phase mixture is given with Eq. (8).

For churn-turbulent flows, a new correlation is proposed

$$C_D = 1.487 D_p \left(\frac{g\Delta\rho}{\sigma}\right)^{1/2} (1 - \varphi)^3 (1 - 0.75\varphi)^2 \tag{12}$$

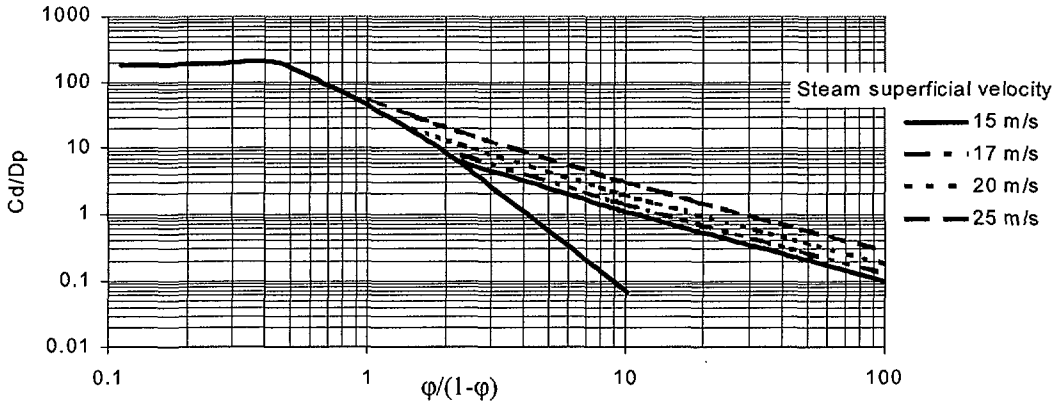

Figure 2 Ratio of interfacial drag coefficient C_D and dispersed particle diameter D_P versus void fraction for two-phase flow within rod bundle at atmospheric conditions

where the dependence on the mixture void fraction φ has the same function form as the CATHARE code correlation [9] for the interface friction in the transitional two-phase flow patterns.

For annular and mist flow patterns, C_D is proportional to the square of the vapour velocity, as proposed in [10]

$$C_D = 7.136 \cdot 10^{-5} D_p \left(\frac{g\Delta\rho}{\sigma} \right)^{1/2} (1-\varphi) u_2^2 \tag{13}$$

The functional dependence of the nondimensional parameter C_D/D_P on the void fraction is given in Fig. 2. For churn-turbulent flow, there is a rapid decrease of the C_D/D_P ratio. This could be attributed to the decrease of the two-phase flow interfacial area concentration, that is to the increase of the dispersed particle diameter D_P (it should be noted that the definition of the D_P for churn-turbulent flow pattern is rather artificial). This decrease of C_D/D_P is slowed for annular and mist flows due to the presence of liquid droplets entrained in the vapour core.

For two-phase flows in free channels, without the volumetric flow resistance, r. h. s. of Eqs. (10), (12) and (13) are divided by 0.4.

The lift force. The lift force acts in the direction perpendicular to the relative velocity, Eq. (14).

$$F_{L2,i} = -C_L \rho_1 \alpha_2 \left[(u_{2,j} - u_{1,j}) \frac{\partial u_{1,j}}{\partial x_i} - (u_{2,j} - u_{1,j}) \frac{\partial u_{1,i}}{\partial x_j} \right] \tag{14}$$

The lift force is mainly caused by the vortex formation around dispersed particle. The lift coefficient C_L depends on the dispersed particle Eötvös number

$$Eo = \frac{g(\rho_1 - \rho_2) D_P^2}{\sigma} \tag{15}$$

For upward bubbly flow and small Eo numbers bubbles will migrate toward the channel walls and $C_L > 0$, while for large Eo numbers bubbles will migrate toward the flow channel center and $C_L < 0$. Various ranges of the lift coefficient values C_L have been reported: 0.5 for inviscid bubbly flow and 0.01 for highly viscous bubbly flow [10], (0.25 – 0.3) for small Eo numbers, while an empirical correlation is proposed in [11]. Calculations with here presented model have shown that the lift force has no practical influence on the void fraction distribution in the forced two-phase flow through a vertical rod bundle. Anyway, the lift force is included for bubble flow patterns and the value of C_L=0.3 is adopted.

The virtual mass force. This force arises in the transient flow due to the force required to accelerate the apparent mass

of surrounding phase when the relative velocity changes. It is important only for very rapid changes in the flow, as in blowdown transient. It is given with

$$F_{VM,i} = C_{VM}\alpha_2\rho_1\left(\frac{\partial u_{2,i}}{\partial t} + u_{2,j}\frac{\partial u_{2,i}}{\partial x_j} - \frac{\partial u_{1,i}}{\partial t} - u_{1,j}\frac{\partial u_{1,i}}{\partial x_j}\right) \tag{16}$$

where the values for C_{VM} are determined for bubbly two-phase flow in the range $1.2<C_{VM}<3.4$ [12].

Tube bundle flow resistance. The pressure drop due to the two-phase mixture flow around rods in a bundle is determined by taking into account the separate contribution of the each phase to the total pressure drop. The pressure drop of the water flow in the $\vec{i}$ coordinate axis direction (i=x,y,z) is

$$\Delta p_{1,i} = \zeta_{1,i}\frac{\rho_1\hat{u}_{1,i}^2}{2}(1-\varphi) \tag{17}$$

where $\zeta_{1,i}$ is the water pressure loss coefficient in the e direction. For the steam phase

$$\Delta p_{2,i} = \zeta_{2,i}\frac{\rho_2\hat{u}_{2,i}^2}{2}\varphi \tag{18}$$

where $\zeta_{2,i}$ is the steam pressure loss coefficient in the i direction. The notation $\hat{u}_{k,i}$, $k=1,2$, denotes the maximum velocity of the phase in e direction, which takes place in the clearance between rods. It is calculated with

$$\hat{u}_{k,i} = u_{k,i}/(1-D/P_i). \tag{19}$$

The above Eq. (19) is derived under the assumption that the void fraction in two-phase mixture φ is the same for all parts of the flow area included in a control volume.

Rod wall–fluid drag force is calculated as follows

$$F_{3k,i} = (1-\alpha_3)\frac{\Delta p_{k,i}}{\Delta e_i} \tag{20}$$

where Δe is the width of the computational cell in the $\vec{i}$ direction (i=x,y,z), and index k=1,2.

Pressure loss coefficients $\zeta_{k,i}$, (k=1,2) are calculated with the correlations recommended in [13].

Interfacial phase change. The intensity of evaporation and condensation rate in two-phase mixture is calculated with the simple empirical model which takes into account the phase change relaxation time (τ). The intensity of evaporation rate is calculated when the water enthalpy is greater than the water saturation enthalpy, i.e. $h_1 > h'$ with the following correlation

$$\Gamma_e = \frac{\alpha_1\rho_1}{\tau}\frac{h_1-h'}{h''-h'}. \tag{21}$$

The condensation within control volume takes place according to the physical condition that the steam is in contact with the subcooled water, i.e. $h_1 < h'$ and $\alpha_2 > 0$. The intensity of condensation rate is calculated with

$$\Gamma_c = \frac{\alpha_1 \rho_1}{\tau} \frac{h' - h_1}{h'' - h'}. \tag{22}$$

Heat rate per unit volume. The volumetric heat rate from rods' walls to the phase k is calculated with

$$\dot{q}'''_{w3k} = \dot{q}_{Ak} a_{i3} \tag{23}$$

where

$$\dot{q}_A = h(T_3 - T_k) \tag{24}$$

and a_{i3} is the interfacial area concentration of tubes/rods outer surface in the unit control volume, that is

$$a_{i3} = \frac{S}{V} \tag{25}$$

where S is the rods' outer surface within the control volume of size V. The heat transfer coefficient from a wall to two-phase mixture in bubbly and churn-turbulent flow is calculated by the correlation recommended for the saturated nucleate boiling [13]

$$h = f(p) q_A^n, \tag{26}$$

where

$$f(p) = 4.32(p^{0.14} + 1.28 \cdot 10^{-2} p^2), \tag{27}$$
$$n = 0.7,$$

and the units applied in Eqs.(26-27) are p (MPa), q (W/m^2). For other two-phase flow patterns and heat transfer regimes the correlations presented in [14] are applied.

5. TURBULENCE MODELLING

Several approaches are developed for turbulent fluid flow simulation and modelling. Some general methods are mentioned here [15,16,17]. The most relevant ones for engineering applications are methods based on the solution of the Reynolds averaged Navier-Stokes equations, in which the turbulent momentum shear stresses are modelled with the Boussinesq's eddy-viscosity concept. This approach introduces the eddy viscosity parameter, which can be determined by turbulence models of different complexity. The most common approach is based on the standard k-ε model and application of the so-called "wall functions" for turbulence parameters prediction in a vicinity of the wall. One way of the k-ε model improvement is the introduction of the low-Reynolds-number turbulence models, which allow the solution of the turbulent kinetic energy and dissipation rate balance equations directly to the wall. The other more complex method is based on the application of the turbulent-stress/flux models, which directly calculates turbulent stress tensor by the solution of higher order turbulence equations. A better physical description of the turbulence flow phenomena is achieved with the large eddy simulation method, where large scale turbulent effects are directly simulated, while the small scale turbulent eddies are modelled with simple sub-grid turbulent models. Introducing a higher level of turbulence modelling realism, more accurate results are obtained, but the engineering applicability of the models is reduced. The most accurate turbulence prediction is achieved with the direct numerical simulation of the turbulent flow by the direct solution of the Navier-Stokes equations, but due to the required computer storage and

calculation time, this approach is restricted to low Reynolds number flows and limited flow domains. This state-of-the-art in turbulence modelling and a need for a greater number of computer simulation runs, in order to evaluate the influence of the spacers geometry on the turbulent flow and recirculation zones structure, have led to the use of the appropriate type of k-ε turbulence model, as the estimated optimum between required accuracy and computer time and memory usage.
The Boussinesq's eddy viscosity concept is applied, which is generalized in the following form

$$-\overline{u_i'u_j'} = \eta_t\left(\frac{\partial u_i}{\partial x_j}+\frac{\partial u_j}{\partial x_i}\right)-\frac{2}{3}k\delta_{ij} \tag{28}$$

for momentum turbulent transport, and for the thermal energy turbulent transport in the form

$$\overline{u_i'T} = \frac{\eta_t}{\mathrm{Pr}_t}\frac{\partial T}{\partial x_i} \tag{29}$$

The momentum and energy conservation equations Eqs. (2-3) for one-phase flow in a free channel without volumetric hydraulic resistance, and with applied Boussinesq's eddy viscosity concept are given in Appendix 1.

The Kolmogorov-Prandtl relation is applied for the eddy viscosity prediction

$$\eta_t = c_\mu\frac{k^2}{\varepsilon} \tag{30}$$

Turbulent kinetic energy and dissipation are predicted by the two-equation k-ε model, which has the following form in Cartesian coordinate system

Turbulence Kinetic Energy Equation

$$\frac{\partial(\rho k)}{\partial t}+\frac{\partial(\rho u_i k)}{\partial x_i}=\frac{\partial}{\partial x_i}\left(\Gamma_k\frac{\partial k}{\partial x_i}\right)+P-\rho\varepsilon \tag{31}$$

Turbulence Dissipation Rate Equation

$$\frac{\partial(\rho\varepsilon)}{\partial t}+\frac{\partial(\rho u_i\varepsilon)}{\partial x_i}=\frac{\partial}{\partial x_i}\left(\Gamma_\varepsilon\frac{\partial\varepsilon}{\partial x_i}\right)+C_{\varepsilon 1}P\frac{\varepsilon}{k}-C_{\varepsilon 2}\rho\frac{\varepsilon^2}{k} \tag{32}$$

where P is the turbulent kinetic energy production

$$P=\rho\eta_t\left[\left(\frac{\partial u_i}{\partial x_j}\right)+\left(\frac{\partial u_j}{\partial x_i}\right)\right]\left(\frac{\partial u_i}{\partial x_j}\right) \tag{33}$$

and diffusion coefficients are given by

$$\Gamma_k=\rho\left(\eta+\frac{\eta_t}{\sigma_k}\right) \tag{34}$$

and

$$\Gamma_\varepsilon=\rho\left(\eta+\frac{\eta_t}{\sigma_\varepsilon}\right) \tag{35}$$

Empirical constants are presented in the following Table.

Table 2: Empirical constants for the standard k-ε model

c_μ	$C_{\varepsilon 1}$	$C_{\varepsilon 2}$	σ_k	σ_ε
0.09	1.44	1.92	1.0	1.3

Turbulence models of two-phase flows are still in the phase of development. The main attempts were directed towards the bubbly flow modelling. Extensions of standard k-ε turbulence model and turbulent-stress/flux models were maid by Lahey and co-workers for bubbly flows [12]. Also, Serizawa and co workers applied mixing length models for bubbly flow modelling [18]. Turbulence phenomena were modeled within a continuous phase, such as liquid film modelling with application of the standard [19] or low-Reynolds number k-ε turbulence models [20] and prediction of k and ε boundary values at the liquid-gas interfaces. General turbulence models for various types of two-phase flow patterns are still not demonstrated. The application of the more general approach is under development by the authors of these papers and promising results are achieved [4].

6. BOUNDARY CONDITIONS

Boundary conditions for the one-phase and two-phase flows depend on the type of the flow channel geometry, as well as on the flow structure, such as turbulent or laminar flow conditions, rigid wall or control volume boundaries etc. As example, in figure 3 boundary conditions that can arise in modelling of two-dimensional coolant flows around spacers are presented. The boundary conditions should be prescribed for the inflow, outflow, upper and lower planes, as well as for the fluid-wall and fluid–spacer interface. Boundary conditions should be sufficient for a unique determination of the velocity, turbulent kinetic energy and turbulent dissipation rate prediction. For the flow channels arrangements presented in Fig. 3, the boundary conditions are prescribed in Table 3. The so-called "wall functions" are applied for the prediction of velocity components and turbulent parameters k and ε in the computational cells adjacent to the wall.

7. NUMERICAL METHOD OF SOLUTION

The control volume based finite difference method [21] is applied for the numerical solution of the set of balance equations (1-3). A pressure-correction equation is derived according to the SIMPLE numerical method [21] from the momentum and mass balance equations. Two-dimensional flow field is discretized with rectangular control volumes of unit width. Two grids are formed, the basic one for the solution of scalar parameter equations, such as pressure-correction equation, and a staggered grid for the solution of the momentum equations (prediction of velocity fields).

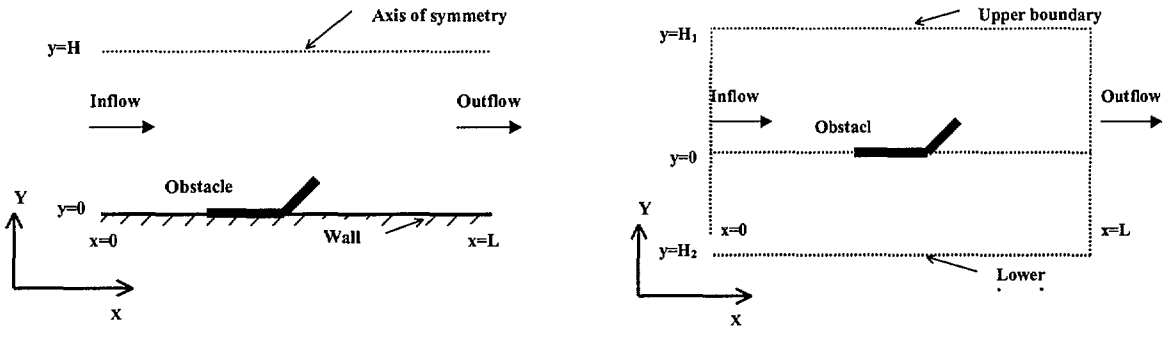

Fig. 3 Flow channel geometry for coolant flow around a spacer mounted on the wall (left) and a spacer in a free stream (right)

A discretization of partial differential equations is carried out by their integration over control volumes of basic and staggered grids.The convection terms are approximated with upwind finite differences, while diffusion and source terms are approximated with central differences. Fully implicit time integration is applied. The resulting set of algebraic equations is solved iteratively with the line-by-line TDMA (Tridiagonal-Matrix Algorithm). For the calculation of a steady-state condition, the transient calculation procedure is performed with constant boundary conditions. General calculation algorithm for transient conditions is presented in Fig. 4, while the calculation scheme applied to the calculation with the k-ε model is presented in Fig. 5. The calculation error for every balance equation and every control volume is kept within prescribed limits by iterative solution of sets of linear algebraic equations. The criterion for the overall calculation procedure solution is the fulfillment of the mass balance for every control volume within prescribed error. Also, this criterion implies that the overall mass balance, for the whole flow field is achieved.

A thickness of the spacer is small in comparison with the flow channel dimensions. Also, the area, which a spacer occupies in a flow channel, is small compared to the whole area. Therefore, from the standpoint of calculation economy it is acceptable to represent the spacers with inactive control volumes, while the whole flow channel area (together with the space occupied with spacers) is covered with the rectangular Cartesian grid (the procedure is clearly stated in [21]). Application of the Cartesian grid with rectangular control volumes has a disadvantage when a spacer's inclined fin is not parallel to the grid lines. Because of this, the fin flat surface must be discretized as a step-wise surface. However, computational results show that this inadequacy has no practical influence on the bulk coolant flow around a spacer. Applied rectangular control volumes can have variable sides; usually control volumes height increases starting from the wall, while it is favourable to increase control volumes length downstream from the spacers.

Table 3: Boundary conditions for flow channels with the spacer mounted on the wall (SW) and the spacer in the free fluid stream (SFS)

Boundary	Flow channel	u	v	k	ε
INLET x = 0	SW	$u = 8/7\overline{u}(y/H)^{1/7}$	$v = 0$	$k = 10^{-4}u^2$	$\varepsilon = k^{3/2}/0.1H$
	SFS	$u = const.$			
OUTLET x = L	SW and SFS	$\frac{\partial u}{\partial x} = 0$	$\frac{\partial v}{\partial x} = 0$	$\frac{\partial k}{\partial x} = 0$	$\frac{\partial \varepsilon}{\partial x} = 0$
AXIS OF SYMMETRY y = H	SW	$\frac{\partial u}{\partial y} = 0$	$\frac{\partial v}{\partial y} = 0$	$\frac{\partial k}{\partial y} = 0$	$\frac{\partial \varepsilon}{\partial y} = 0$
UPPER/LOWER BOUNDARY IN FREE STREAM $y = H_1$, $y = H_2$	SFS	$\frac{\partial u}{\partial y} = 0$	$\frac{\partial v}{\partial y} = 0$	$\frac{\partial k}{\partial y} = 0$	$\frac{\partial \varepsilon}{\partial y} = 0$
FLUID-WALL /SPACER INTERFACE (parameters are calculated for computational cells adjacent to the wall/spacer, boundary conditions for velocity predictions are given for case when u-component is parallel to the wall and v-component is perpendicular to the wall)	SW and SFS	$\frac{u}{u_\tau} = \frac{1}{\kappa}\ln(Ey^+)$, *where* $u_\tau = \sqrt{\frac{\tau_w}{\rho}}$ $\tau_w = \frac{\kappa c_\mu^{1/4}\rho k^{1/2}u}{\ln(Ey^+)}$ $y^+ = \frac{u_\tau y}{\nu}$ $\kappa = 0.4,\ E = 8.8$	$\frac{\partial v}{\partial n} = 0$	$\frac{\partial k}{\partial n} = 0$	$\varepsilon = \frac{c_\mu^{3/4}k^{3/2}}{\kappa y}$

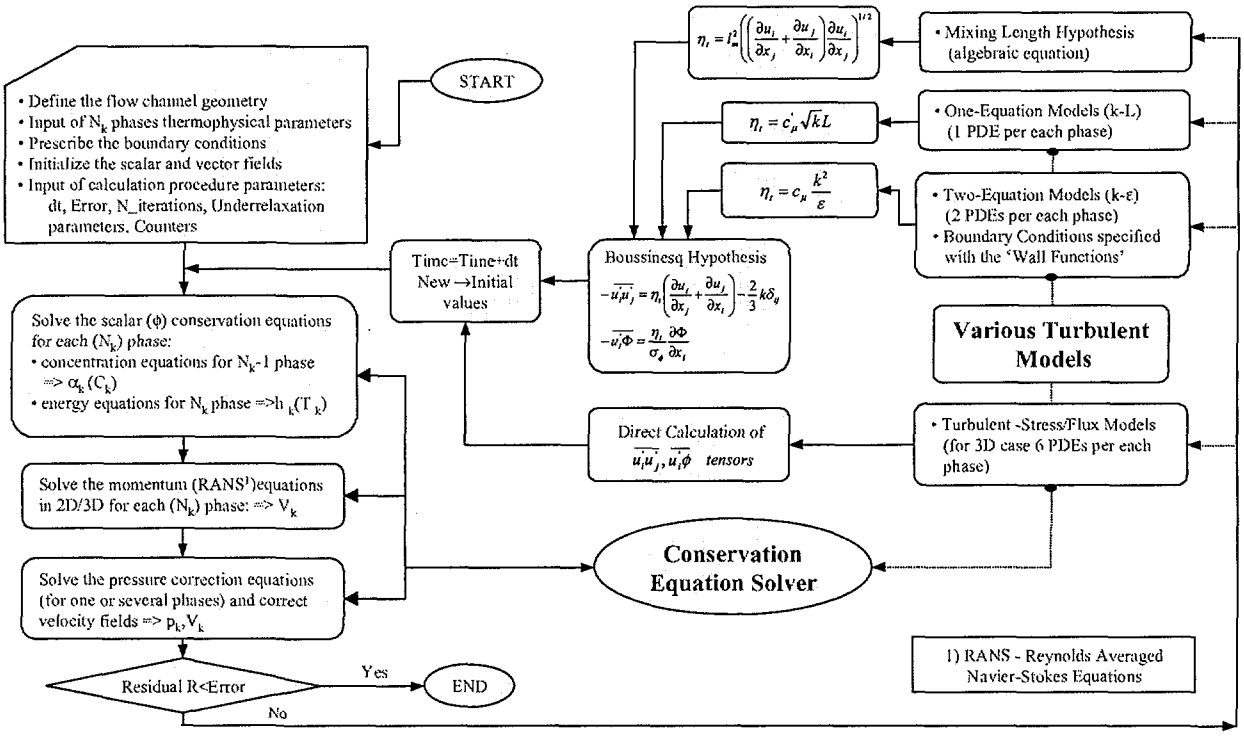

Fig. 4 General calculation procedure for the application of various types of turbulence models

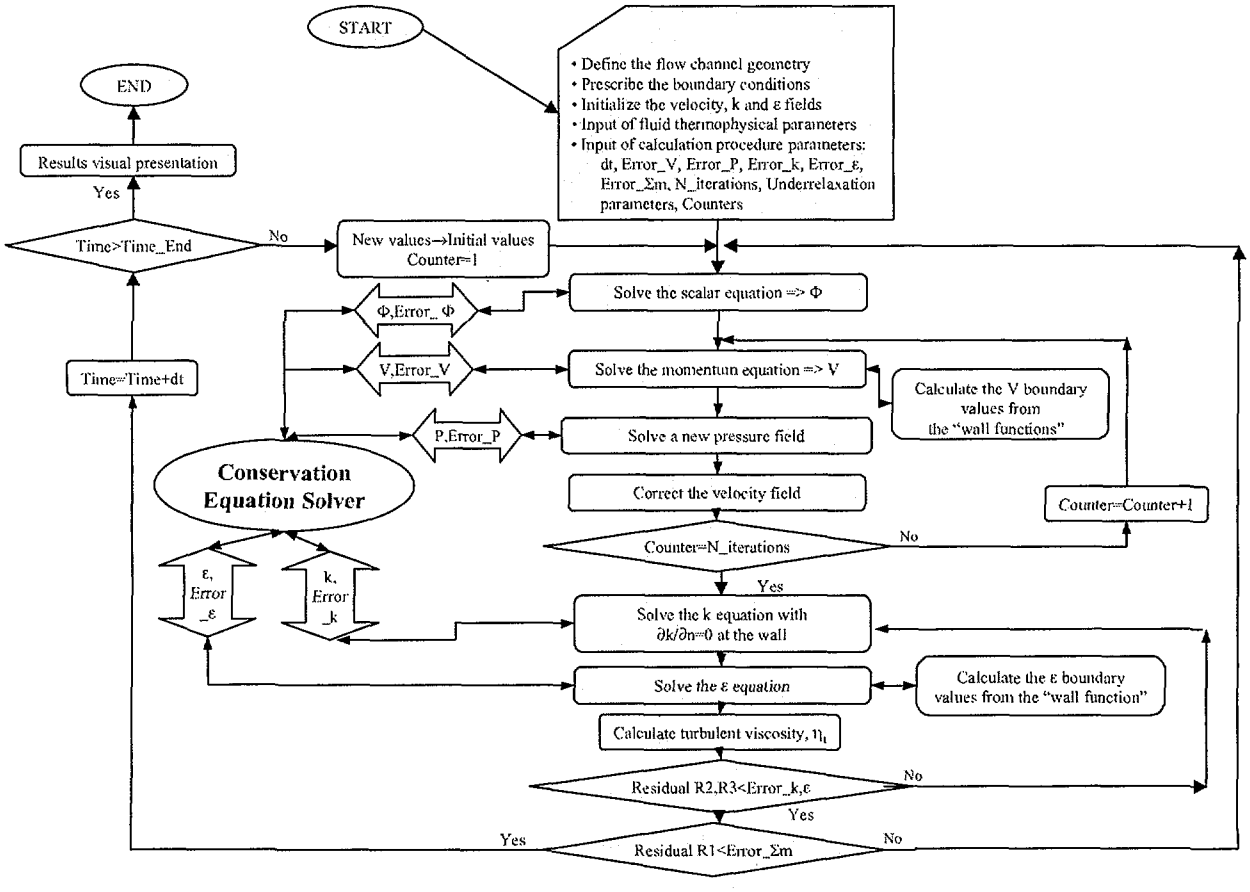

Fig. 5 Calculation flow chart for non-stationary conditions

8. SAMPLE PROBLEMS

Presented model was first used for the simulation of some benchmark tests for two-dimensional fluid flow with recirculation. Later, the model was used for the calculation of coolant flow over spacers with different fin inclinations and for flow over a row of spacers. Some of the results are presented in this paper.

Figure 6 shows calculated velocity vectors and streamlines for air flow over a backward-facing step. Experimental data on this flow condition are reported in [22]. Although the standard k-ε model is used for the turbulent recirculating flow simulation, an acceptable agreement between calculated and measured reattachment length is obtained with an error of 6%. According to [15] the main reason for the standard k-ε model underprediction of the reattachment length is inaccurate prediction of normal Reynolds stress differences in the recirculation zone. Figure 7 shows corresponding pressure field.

Figure 8 shows an example of the simulation of turbulent coolant flow over three spacers mounted on the wall in a row. Dynamic characteristics of recirculation zones interference are shown. Detailed investigation of the coolant flow over spacers is presented in reference [3].

A group of physical experiments was performed with the ATRIUM 10 fuel bundle in order to measure the Critical Power (CP) for steady-state conditions, Fig. 10. These experiments are also simulated and analysed with the here proposed numerical method. Figure 11 shows steam void fraction distribution within the rod bundle at the condition of CP. The influence of spacers is clearly seen. Void fractions are higher in front of the spacers, while at the spacers and downstream the void fraction decreases. According to the temperature measurements, the rod numbered 87 first experienced the dry-out. Numerical simulations also show that the dry-out occurs at the same rod No. 87, Fig. 12.

The occurrence of the dry-out for void equal or greater than 0.95 is shown in front of the last spacer grid and at the rod exit. The two-phase mixture flow redistribution within the rod bundle is shown in Fig. 13. The flow mass flux is increased above the part-length rods, in the upper part of the bundle, due to the reduced flow resistance in these areas.

Also, the lower mass flow rates coincide with the position of the rod No. 87, which experiences dry-out.

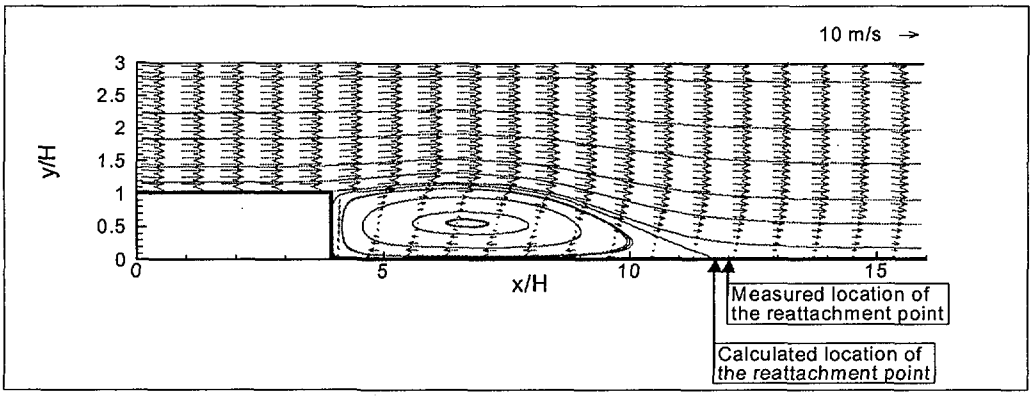

Fig. 6 k-ε model prediction of velocity field and streamlines for air flow over backward-facing step (uniform inlet air velocity is 12 m/s, backward-facing step height is 40 mm, inlet turbulent intensity Tu is 1.41%, predicted reattachment length is 7.6 x_r/H, measured reattachment length for Tu=1.3% is 8.1 x_r/H [22]). A uniform numerical grid with 80x30 control volumes is used.

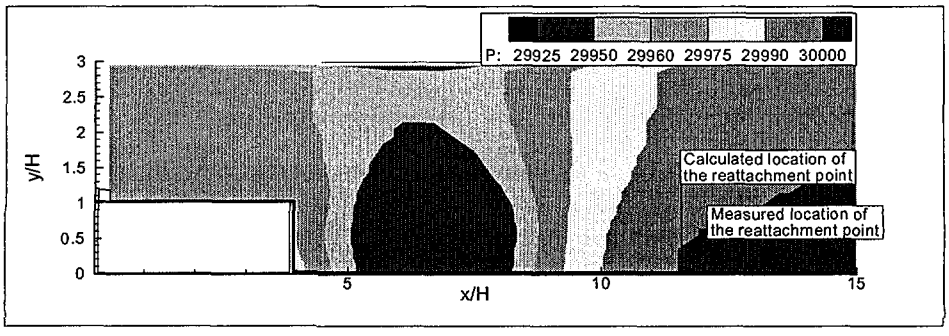

Fig. 7 k-ε model prediction of pressure field for air flow over backward-facing step

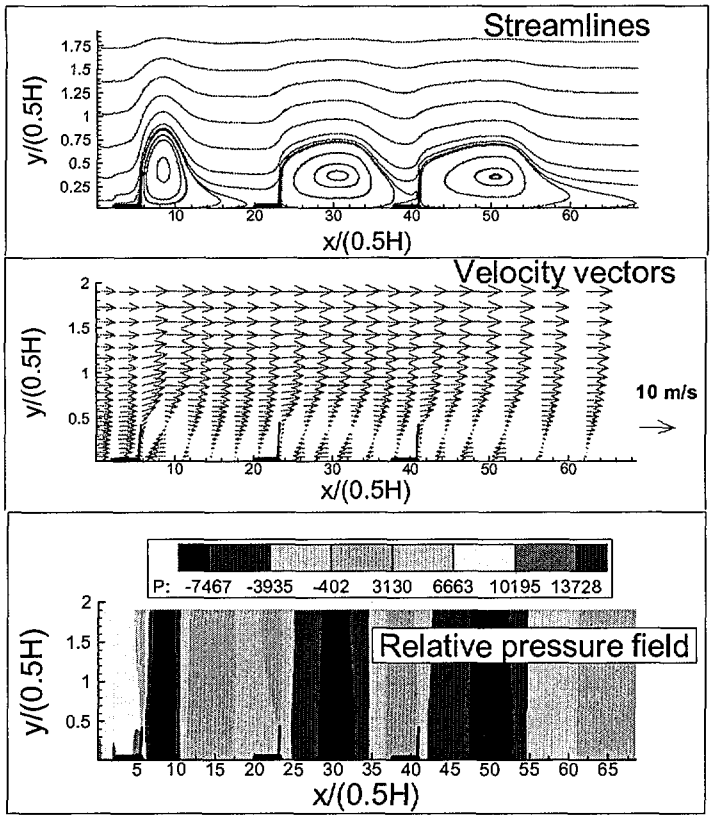

Fig. 9 Water flow over three spacers in a row. The width of the upstream recirculation zone is suppressed by the downstream spacer. This influence is more pronounced at the first spacer and less at the second one. The calculation is performed with the 600x24 control volumes with variable size (control volumes height increases from the wall to the upper axis of symmetry, while control volumes length increases after the third spacer up to the channel exit). All three spacers' fins are 60^0 inclined to the wall. Channel width H is 0.0204 mm and length 0.7 m. Water density is 760 kg/m^3.

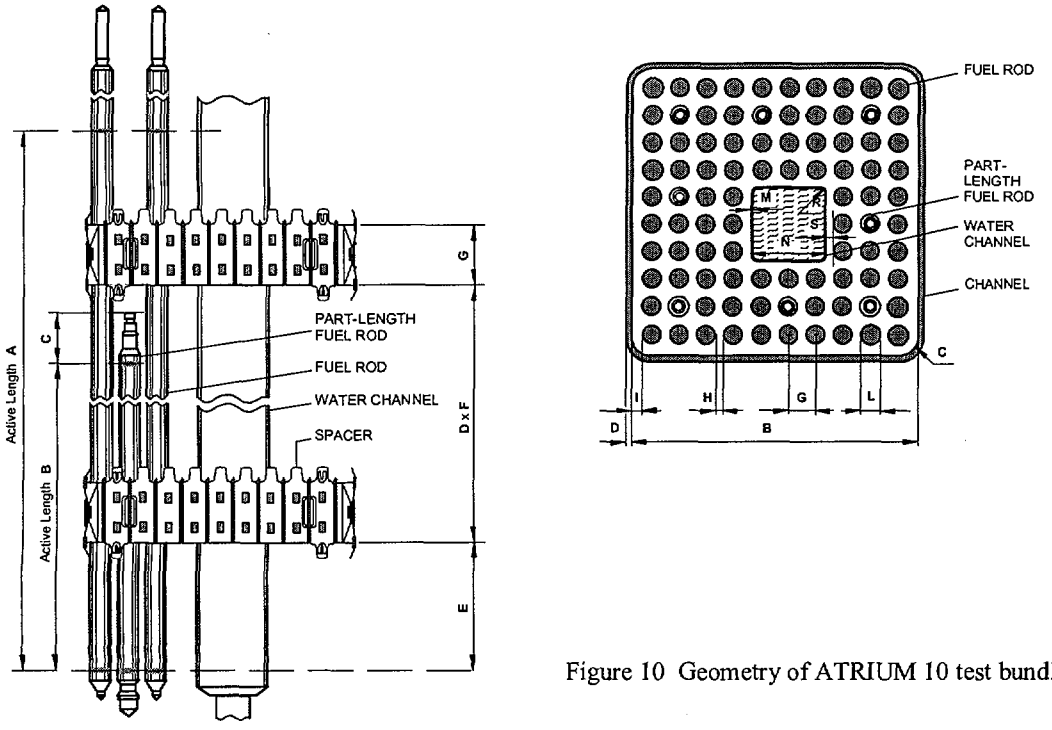

Figure 10 Geometry of ATRIUM 10 test bundle

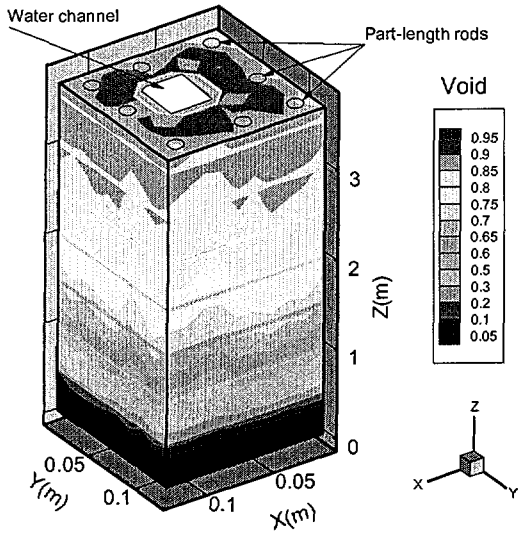

Figure 11 Steam void fraction distribution within the ATRIUM 10 nuclear fuel rod bundle under Dyout condition (mass flow rate 16 kg/s, inlet subcooling 35.5 kJ/kg)

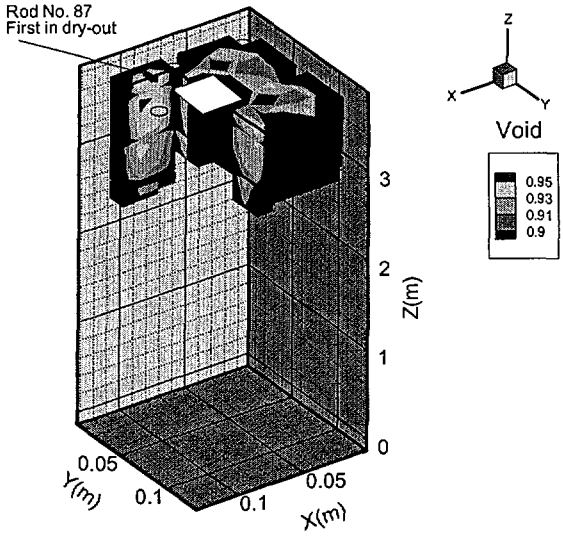

Figure 12 Steam void fraction exceeds the value of the 0.95 leading to Dryout at Rod No. 87 (mass flow rate 16 kg/s, inlet subcooling 35.5 kJ/kg)

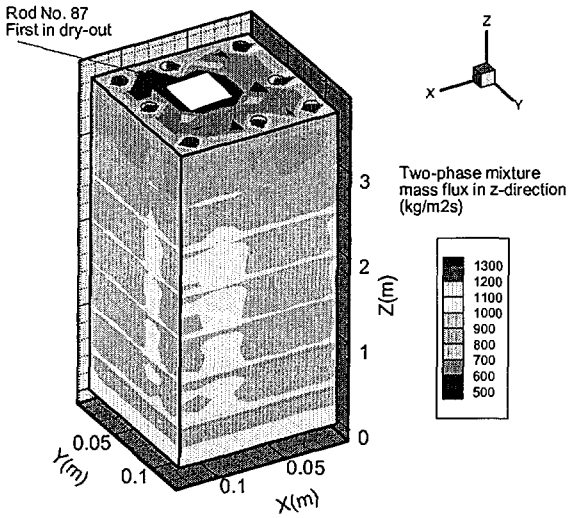

Figure 13 Two-phase mixture flow redistribution within the ATRIUM 10 fuel rod bundle (mass flow rate 16 kg/s, inlet subcooling 35.5 kJ/kg)

9. CONCLUSION

The methodology for the simulation and analysis of turbulent coolant flow around one or several spacers in a row is presented, based on the control volume solution of the governing equations, appropriate k-ε model, and on the application of the 'wall functions". Results of sample problems solutions are included: an air flow over backward-facing step, a coolant flow over a row of three spacers and two-phase flow within a rod bundle. The stated methodology is an effective tool for the investigation of one-phase and two-phase coolant flow around nuclear fuel spacers of various geometry and spatial arrangements.

REFERENCES

[1] Stosic, Z., *The Rod Bundle Spacer Grid Effects on Post-Dryout Heat Transfer Augmentation Analysed by the model HECHAN 2.1.* 4th ASME/JSME Thermal Engineering Joint Conference, Maui, Hawaii, USA, March 19-24, 1995.

[2] Stosic, Z., *On the Role of Spacer Grids on Conditions of Dryout/Rewetting on local Thermal Hydraulics in Boiling Water Channels*, 9th International Topical Meeting on Nuclear Reactor Thermal Hydraulics – NURETH-9, San Fracisco, Ca, USA, October 3-9, 1999.

[3] Stosic, Z., Stevanovic, V., *Analytical investigation of the influence of spacer geometry and position on turbulent flow structure and parameters*, International Conference on Nuclear Engineering – ICONE 9, Nice, 2001.

[4] Stosic, Z., Stevanovic, V., *The influence of the spacer's fin angle on the two-phase flow separation*, Submitted to Int. J. Multiphase Flow, 2001.

[5] Ishii, M., *Two-fluid Model for Two-phase Flow*, Presented at the 2nd Int. Workshop on Two-Phase Flow Fundamentals, Proc. 2nd Int. Workshop on Two-Phase Flow Fundamentals, Rensselaer Polytechnic Institute, Troy NY, 1987.

[6] Dukler, A. E., Taitel, Y., *Flow Pattern transition in Gas-Liquid Systems: Measurements and Modelling*, Multiphase Science and Technology, Vol. 2, Hemisphere Publ. Co., 1986.

[7] Kuznecov, Yu. N., *Heat Transfer in Problems of the Nuclear Reactors Safety*, Energoatomizdat, Moscow, 1989 (in Russian).

[8] Ishii, M., Zuber, N., *Drag Coefficient and Relative Velocity in Bubbly, Droplet or Particulate Flows*, AIChE Journal, vol. 25, pp. 843-855, 1979.

[9] Rousseau, J. C, Houdayer, G., *Advanced Safety Code CATHARE Summary of Verification Studies on Separate Effects Experiments*, Proc. Nuclear Reactor Thermal-Hydraulics NURETH 2, 1983.

[10] Lahey, R. T., *The Analysis of Phase Separation and Phase Distribution Phenomena using Two-Fluid Models*, 3rd Int. Topical Meeting on Nuclear Power Plant Thermal-Hydraulics and Operation, Seul, Korea, November, 1988, pp. A1-69-87.

[11] Tomiyama, A., *Struggle with Computational Bubble Dynamics*, 3rd Int. Conf. On Multiphase Flow, Lyon, France, June 8-12, 1998.

[12] Lopez de Bertodano, M., Lahey., R.T., Jones, O., *Phase Distribution in Bubbly Two-Phase Flow in Vertical Ducts*, Int. J. Multiphase Flow, Vol. 20, No. 5, pp. 805-818, 1994.

[13] Rassohin, N. G., *Nuclear Power Plants Steam Generators*, Moskva, Atomizdat, 1980. pp. 106, (in Russian).

[14] Stosic, Z., *Study on Thermal Performance and Margins of BWR Fuel Elements*, 7th Int. Conf. On Nuclear Engineering, Tokyo, Japan, April 19-23, 1999.

[15] Speziale, C. G., *Modelling of Turbulent Transport Equations, in Simulation and Modelling of Turbulent Flows*, Edited by T. B. Gatski, M. Y. Hussaini, J. L. Lumley, Oxford University Press, 1996.

[16] Rodi, W., *Turbulence Models and Their Application in Hydraulics*, IAHR Monograph, A. A. Balkema Publishers, Rotterdam, 1993.

[17] Belov, S. A. Isaev, Korobkov, V. A., *Problems and Methods of Calculating incompressible fluid motions with flow separation*, Sudostroenie, Sankt Petersburg, 1989. (in Russian)

[18] Kataoka, I., Serizawa, A., *Modelling and Prediction of Turbulence in Bubbly Two-Phase Flow*, Proceeding of the 2nd Int. Conference on Multiphase Flow, Kyoto, 1995.

[19] Lorencez, C., Nasr-Esfahany, M., Kawaji, M., Ojha, M., *Liquid Turbulence at a Sheared and Wavy Gas-Liquid Interface*, Int. J. Multiphase Flow, Vol. 23, No. 2, pp. 205-226, 1997.

[20] Stevanovic, V., *Modelling of Condensation in Steam-Water Stratified Flow Based on Convective Heat Transfer*, Proceedings of the 4th International Conference on Nuclear Engineering, ICONE-4, Vol.1, New Orleans, 1996.

[21] Patankar, S. V., *Numerical Heat Transfer and Fluid Flow*, Hemisphere, 1980.

[22] Isomoto, K., Honami, S., *The Effect of Inlet Turbulence Intensity on the Reattachment Process Over Backward Facing Step*, Journal of Fluids Engineering, Vol. 111, pp. 87-92, 1989.

Appendix 1

The following momentum conservation equations are derived in two-dimensions

$$\frac{\partial(\rho u)}{\partial t}+\frac{\partial(\rho u^2)}{\partial x}+\frac{\partial(\rho uv)}{\partial y}= -\frac{\partial p}{\partial x}+\frac{\partial}{\partial x}\left[(\rho\eta_e)\frac{\partial u}{\partial x}\right]+\frac{\partial}{\partial y}\left[(\rho\eta_e)\frac{\partial u}{\partial y}\right]+\frac{\partial}{\partial x}\left[\rho\eta_t\frac{\partial u}{\partial x}\right]+\frac{\partial}{\partial y}\left[\rho\eta_t\frac{\partial v}{\partial x}\right]-\frac{2}{3}\frac{\partial(\rho k)}{\partial x} \tag{A1-1}$$

$$\frac{\partial(\rho v)}{\partial t}+\frac{\partial(\rho uv)}{\partial x}+\frac{\partial(\rho v^2)}{\partial y}= -\frac{\partial p}{\partial y}+\frac{\partial}{\partial x}\left[(\rho\eta_e)\frac{\partial v}{\partial x}\right]+\frac{\partial}{\partial y}\left[(\rho\eta_e)\frac{\partial v}{\partial y}\right]+\frac{\partial}{\partial x}\left[\rho\eta_t\frac{\partial u}{\partial y}\right]+\frac{\partial}{\partial y}\left[\rho\eta_t\frac{\partial v}{\partial y}\right]-\frac{2}{3}\frac{\partial(\rho k)}{\partial y} \tag{A1-2}$$

where the effective kinematic viscosity is the sum of the laminar and turbulent values

$$\eta_e=\eta+\eta_t \tag{A1-3}$$

The scalar parameter balance equation for two-dimensional flow conditions takes the following form with the application of the eddy-diffusivity concept

$$\frac{\partial(\rho h)}{\partial t}+\frac{\partial(\rho uh)}{\partial x}+\frac{\partial(\rho uh)}{\partial y}=\frac{\partial}{\partial x}\left[k_{eff}\frac{\partial T}{\partial x}\right]+\frac{\partial}{\partial y}\left[k_{eff}\frac{\partial T}{\partial y}\right]+\dot{q}''' \tag{A1-4}$$

where the effective diffusion coefficient is

$$k_{eff}=k+\rho c_p\frac{\nu_t}{\mathrm{Pr}_t} \tag{A1-5}$$

and Pr_t is the turbulent Prandtl number.

The extension of the balance equations (8), (9) and (11) to three-dimensional problems is straightforward by adding corresponding convection terms on the left hand sides and diffusion terms on the r. h. s. of these equations.